PUBLISHED VERSION

B. M. Sparkes, M. Hosseini, C. Cairns, D. Higginbottom, G. T. Campbell, P. K. Lam, and B. C. Buchler
Precision spectral manipulation: a demonstration using a coherent optical memory
Physical Review X, 2012; 2(2):021011-1-021011-10

Originally published at:
http://doi.org/10.1103/PhysRevX.2.021011

PERMISSIONS

http://creativecommons.org/licenses/by/3.0/

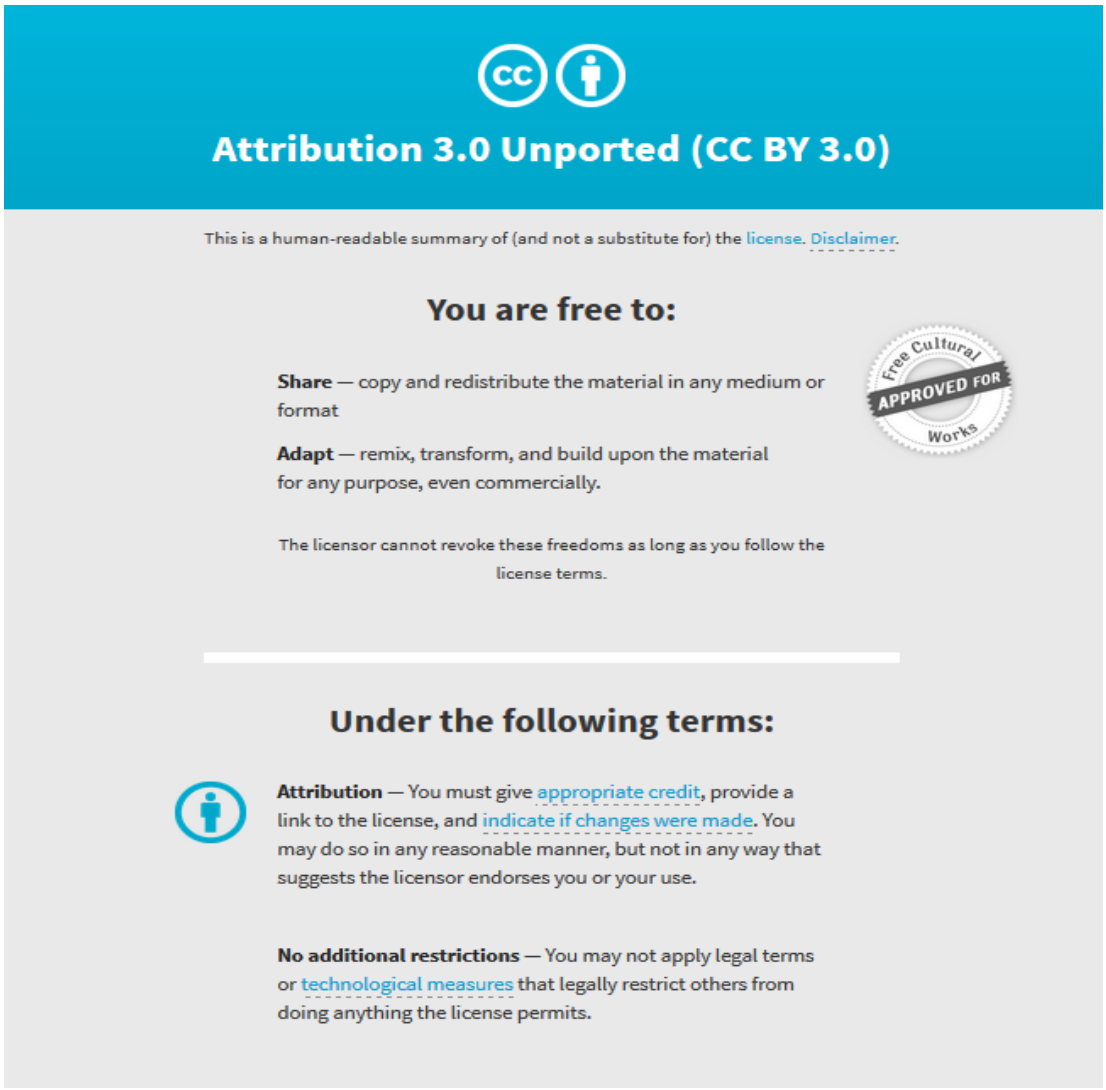

4 July 2017

Precision Spectral Manipulation: A Demonstration Using a Coherent Optical Memory

B. M. Sparkes, M. Hosseini, C. Cairns, D. Higginbottom, G. T. Campbell, P. K. Lam, and B. C. Buchler

Centre for Quantum Computation and Communication Technology, Department of Quantum Science, Research School of Physics and Engineering, The Australian National University, Canberra, ACT 0200, Australia

(Received 22 February 2012; published 20 June 2012)

The ability to coherently spectrally manipulate quantum information has the potential to improve qubit rates across quantum channels and find applications in optical quantum computing. In this paper, we present experiments that use a multielement solenoid combined with the three-level gradient echo memory scheme to perform precision spectral manipulation of optical pulses. These operations include separate bandwidth and frequency manipulation with precision down to tens of kHz, spectral filtering of up to three separate frequency components, as well as time-delayed interference between pulses with both the same, and different, frequencies. If applied in a quantum information network, these operations would enable frequency-based multiplexing of qubits.

DOI: 10.1103/PhysRevX.2.021011 Subject Areas: Atomic and Molecular Physics, Quantum Physics, Quantum Information

I. INTRODUCTION

Quantum information processing seeks to harness quantum mechanics to enhance information processing capabilities. Just as classical communication and computation require memory buffers, quantum information systems will require memories for quantum states. An optical quantum memory allows coherent, noiseless, and efficient storage and recall of optical quantum states. They are an essential building block for quantum repeaters [1], which will extend the range of quantum communication. Optical quantum states could also find applications as a synchronization tool for optical quantum computers, and in deterministic single-photon sources [2]. Much progress has been achieved toward this goal in recent years, with efficiencies up to 87% [3], storage times of over 1 s [4,5], as well as bandwidths above a gigahertz [6,7] and over 1000 pulses stored at once [8], all being separately demonstrated using different storage techniques.

In addition to memories, a method for conditioning qubits in terms of their timing, frequency, and bandwidth would be another useful component of a quantum communication system. The ability to coherently manipulate the spectrum of pulses would prove a key tool for allowing quantum information transfer between systems with different bandwidths. This ability could lead to increased bit rates over quantum communication channels [9]. Being able to alter a pulse's shape, as well as its bandwidth, could also lead to increased bit rates due to a decrease in losses caused by pulse aberrations through various media (i.e., optical fiber [10]). There are numerous options available for conditioning operations, some of which would be suitable for quantum information applications. Diffraction techniques [11], electro-optic modulators [12–14], and acousto-optic modulators [15] have been used to modulate pulse amplitude and phase, as well as pulse compression and shaping. Spatial light modulators can also be used to shape both classical [16] and quantum [17–19] pulses. Another classical tool is temporal-lensing systems [20], which can be used to compress [21,22] and expand [23] pulses, as well as perform time-to-frequency conversion [24,25]. Four-wave mixing can also be used to alter the frequency of a pulse (for examples, see Refs. [26,27]). In addition to these, there are quantum techniques that can be used to manipulate pulses. For instance, three-wave mixing [28], quantum-pulse gates [29,30], and pulsed frequency up- [31–33] and down-conversion [34,35] have all been shown to be able to coherently alter either the temporal or spectral profile of optical pulses. Frequency up-conversion has also been used as the basis of an optical switch [36].

Given that a memory will already be a part of a quantum information network, an enticing possibility is that qubit conditioning could be built into the memory functionality. If this is possible, it would not only save the addition of extra components (and the extra loss and complexity this entails) but would also allow dynamic programming of the manipulation and timing—as the information would not simply be passing through the system, but trapped. It could also allow for controllable multiplexing within the memories—a powerful tool where multiple signals are bundled into one over a communication channel. Multiplexing could be achieved with, for instance, different spatial [37], temporal [38], or frequency modes in a quantum memory. Being able to perform multiplexing with a quantum memory has also been suggested as a way of improving quantum-repeater designs by speeding up the entanglement-generation process [38] and reducing their sensitivity to memory coherence times [39].

Electromagnetically induced transparency-based memory has been investigated with respect to pulse shaping and

splitting inside a coherent memory [40,41], although with efficiencies limited to below 50%. By introducing a second counterpropagating coupling field, an electromagnetically induced grating can be created, allowing for optical switching and routing [42], as well as positioning [43]. The manipulation of stored information has also been demonstrated in photon-echo-based quantum memories. For instance, the ability to perform spectral manipulation using a modified photon-echo scheme has been shown theoretically [44] and, using the three-pulse photon echo, interference between two pulses has been experimentally demonstrated [45].

In this paper, we investigate the coherent spectral manipulation abilities of the three-level gradient echo memory (Λ GEM) scheme [46–48]. GEM is a photon-echo-based quantum memory that has been shown to have high efficiencies in both its two-level [49] and three-level [3] forms, which are based on rare-earth ions and atomic gases, respectively. Both forms have been shown not to add noise to the quantum state [49,50], therefore performing above the no-cloning limit, making GEM a promising candidate as an optical quantum memory.

Previous experimental work on Λ GEM has shown that it is capable of storing up to 20 pulses simultaneously [3] and is able to manipulate stored light in a number of ways: It has been used to resequence pulses, stretch or compress the bandwidth of stored pulses [51], add a frequency offset to the recalled light [3], and interfere two pulses within the memory [52]. Modeling has shown that GEM schemes are capable of much more. For example, a GEM scheme could be used as an optical router [53] or an all-optical multiplexer [54]. In this paper, we investigate, in detail, proposals that make particular use of the frequency-encoding nature of GEM to coherently manipulate the spectrum of stored pulses, filter modulated pulses, and combine or interfere pulses of different frequencies [55]. Using our memory, we also demonstrate the feasibility of frequency multiplexing where we can independently store and recall pulses of different frequencies.

The remainder of this paper is structured as follows: Section II presents an overview of the GEM protocol and relevant theory before we describe the experimental details in Sec. III. Section IV presents experimental results characterizing basic frequency-manipulation operations, as well as demonstrating frequency-domain engineering with precision control of magnetic-field gradients provided by a multielement coil. Sections V and VI contain discussions and conclusions.

II. GRADIENT ECHO MEMORY OVERVIEW

A linearly varying frequency gradient placed along an ensemble of absorbing atoms is the key component of the gradient echo memory scheme. The detuning of each atom from its original resonance, and therefore the frequency it will absorb, is proportional to its position along the memory. Therefore, GEM is a frequency-encoding memory, with pulses being stored as their spatial Fourier transform along the memory. For a linear gradient, $\eta(z) = \eta$, the bandwidth of the memory is determined by $\mathcal{B}_s = \eta l$, where l is the memory length. We assume here that the center-pulse frequency ω_c is stored in the middle of the memory.

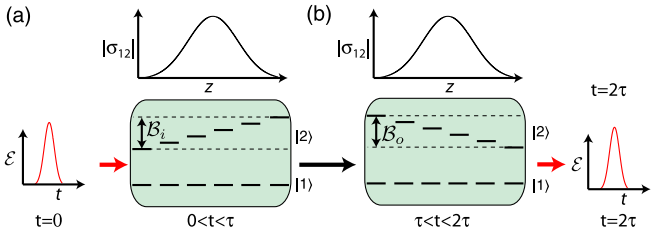

FIG. 1. Basic two-level gradient echo memory operation. (a) A pulse with an input Gaussian envelope $\mathcal{E}_i(t)$, bandwidth $\mathcal{B}_p$, and center frequency ω_{ci} enters the storage medium, at time $t = 0$, where the optical information is stored in the atomic excitation σ_{12}. The memory has a linear frequency gradient placed along it in the z direction and a input frequency bandwidth $\mathcal{B}_i$. (b) At time $t = \tau$, the sign of the frequency gradient is reversed, with the memory output bandwidth $\mathcal{B}_o = \mathcal{B}_i$. In this scheme, the echo is emitted at time $t = 2\tau$ with pulse shape $\mathcal{E}_o(t) = \mathcal{E}_i(-t)$ and center frequency $\omega_{co} = \omega_{ci}$.

The operation of the GEM scheme is shown in Fig. 1. The varying detuning of the atomic absorption frequency is linear as a function of z. Whether discussing a two- or three-level GEM, it is generally sufficient to consider only two levels. In the case of three-level Λ GEM, the excited state can be adiabatically eliminated [56], allowing us to treat the storage mechanism as a quasi-two-level system. The equations that govern the storage of a light pulse with a slowly varying envelope operator $\hat{\mathcal{E}}(z, t)$ inside a two-level ensemble with an atomic polarization operator $\hat{\sigma}_{12} \equiv |1\rangle\langle 2|$ in this situation are [46]

$$\partial_t \hat{\sigma}_{12} = -[\gamma + i\eta(z)]\hat{\sigma}_{12} + ig\hat{\mathcal{E}}, \quad \partial_z \hat{\mathcal{E}} = i\frac{gN}{c}\hat{\sigma}_{12}, \quad (1)$$

where γ is the decay rate from the excited state $|2\rangle$, g is the coupling strength between the two levels, N is the number of atoms, and c is the speed of light. This equation assumes a weak probe field such that $\langle\sigma_{11}\rangle \approx 1$ holds, and that all atoms are initially in this ground state. The three-level system, where a strong classical field is used to couple the two ground states, is equivalent to the two-level system as long as (i) the one-photon detuning $|\Delta| \gg d\gamma$ and (ii) $1 \ll dT\gamma$ [57], where d is the on-resonance optical depth of the system, γ is the excited-state decay rate, and T is the fastest time scale of the system. This equivalence is shown in Fig. 2 (inset). The coupling strength of the equivalent two-level system is given by $g' = g\Omega_c/\Delta$, where Ω_c is the Rabi frequency of the coupling field. The advantage of the Λ system is that the storage time of the memory is now controlled by the ground-state decoherence rate γ_0, which is much less than the excited-state

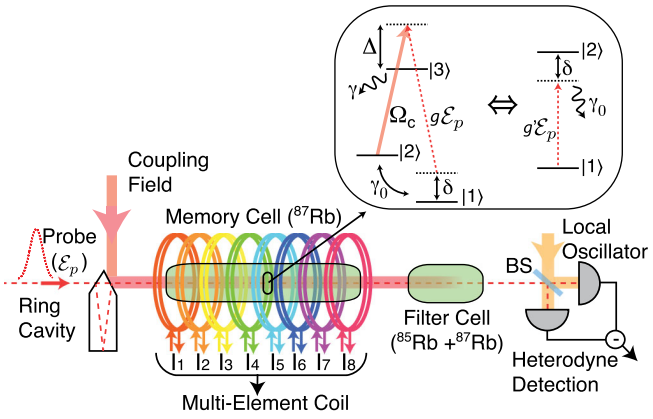

FIG. 2. Experimental setup. Probe electric field envelope ($\mathcal{E}_p$), nonpolarizing beam splitter (BS), and I_1–I_8 currents supplied to the individual solenoids. The inset shows the level scheme and the equivalence between the Λ system used and a two-level atom: one-photon detuning (Δ), two-photon detuning (δ), coupling-field Rabi frequency (Ω_c), decay rate from the excited state (γ), decoherence rate between the ground states (γ_0), coupling strength between ground and excited states (g), and the effective coupling strength for the equivalent two-level system (g').

lifetime. Indeed, there are a wide range of atoms with stable ground-state configurations that are suitable for Λ GEM.

To recall the pulse, under a normal GEM operation, the linear gradient is exactly reversed at a time τ after the pulse has entered the memory, i.e., $\eta(t<\tau) = -\eta(t>\tau)$. This leads to a time reversal of the absorption process described in Eq. (1) and an emission of a time-reversed copy of the input pulse in the forward direction, i.e., $\hat{\mathcal{E}}_o(t) = \hat{\mathcal{E}}_i(2\tau - t)$, at time $t = 2\tau$, with the center frequency of the echo being the same as that of the input pulse.

It is not necessary, however, to recall with an exact reversal of the input gradient to produce an echo, or to have a constant gradient along the entire length of the memory. Indeed, having fine control of the input and output gradients, as discussed in the following sections, is what provides us with the ability to perform spectral manipulation operations using GEM.

III. EXPERIMENTAL SETUP

An overview of the setup used for the following spectral manipulation experiments is shown in Fig. 2. We use the Λ GEM scheme and warm ^{87}Rb vapor for our experiments. The weak probe and strong coupling fields are derived from the same laser, which is blue detuned by approximately 3 GHz from the $F = 2 \rightarrow F' = 2$ ^{87}Rb D_1 transition. A small part of the laser is sent through a fiber-coupled electro-optic modulator driven at 6.8 GHz, the ground-state splitting of ^{87}Rb, and the positive sideband selected by passing it through a filtering cavity. This field, now 3 GHz blue, detuned from the $F = 1 \rightarrow F' = 2$ transition, is used for both the probe and the local oscillator (LO). The probe and coupling fields, having the same circular polarization, are combined on a ring cavity that is resonant with the probe. The probe and coupling fields then enter the memory—a 25-mm-diam, 20-cm-long gas cell containing isotopically enhanced ^{87}Rb, and 0.5-Torr krypton buffer gas, heated to approximately 80 °C using an electronic filament heater.

Eight separate solenoid coils, with four turns each, are placed along the length of the memory. This multielement coil (MEC) is used to create the complex gradients for the experiments, discussed in the following sections, by placing a different current in each coil, and using the superposition principle for magnetic fields, i.e., $B_{\rm tot}(z) = \sum_i B_i(z)$. The two-photon detuning of each atom can then be defined as a function of position along the memory $\delta(z) = 2g_F B_{\rm tot}(z) - \delta_o$, where $g_F = 0.7$ MHz/G is the Landé factor and δ_o is an arbitrary two-photon offset. For instance, in this case, $\delta_o = 0$ is defined for a set dc magnetic-field and coupling-field frequency. The memory cell and coils are surrounded with a layer of μ metal to shield against external magnetic fields. The heater is turned off during the storage process to ensure there are no stray magnetic fields interacting with the atoms.

Upon leaving the memory, the probe and coupling fields pass through a filter cell containing a natural mixture of Rb (i.e., ^{85}Rb and ^{87}Rb), which is heated to approximately 150 °C. Because of the detunings chosen above, the coupling field is resonant with a ^{85}Rb transition, leading to approximately 40-dB suppression through the cell. The probe field, which passes through the filter cell with 70% efficiency, is then combined with the local oscillator signal on a nonpolarizing beam splitter, and heterodyne detection is performed. Fine control of the frequencies of all fields, as well as gating of the probe and coupling fields, is achieved using acousto-optic modulators. This experiment is controlled with an augmented version of the LabVIEW code presented in Ref. [58].

IV. SPECTRAL MANIPULATION EXPERIMENTS

In this section, we first characterize center-frequency and bandwidth manipulations, already demonstrated in proof of principle in previous papers [3,51], using the added control over the magnetic field provided by the MEC. We then present other spectral manipulation results including spectral filtering and pulse interference.

A. Center frequency manipulation

By adding an offset to the recall field, i.e., $\delta(z, t > \tau) = -\delta(z, t < \tau) + \delta_{\rm os}$, the center frequency of the echo relative to the input can be altered and will be given by

$$\omega_{co} = \omega_{ci} \pm \delta_{\rm os}. \tag{2}$$

The sign of $\delta_{\rm os}$ is dependent on which ground state is used. In this case, it is the $|F = 1, m_F = 1\rangle$ state and therefore the sign is negative.

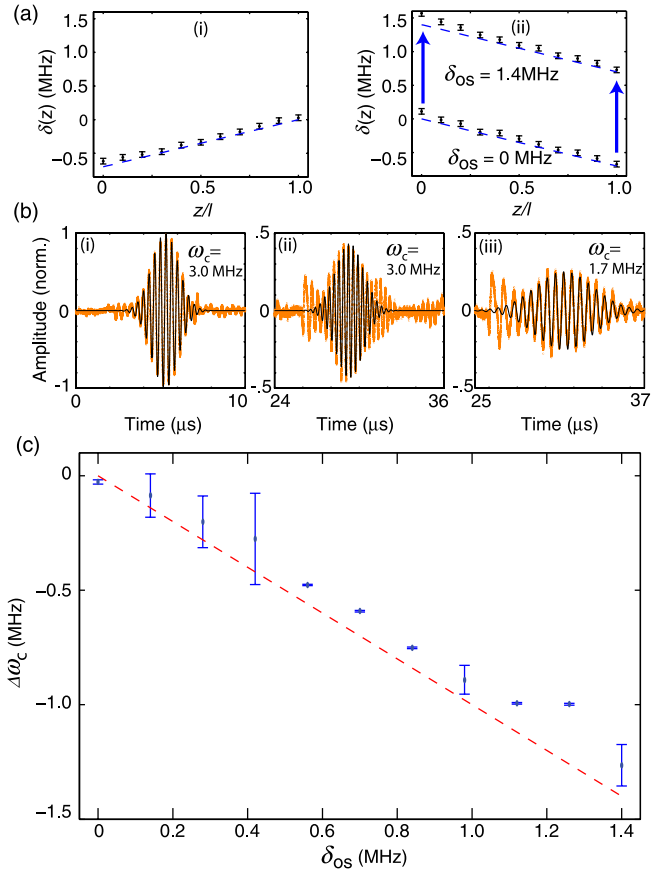

FIG. 3. Manipulating pulse frequency. (a) Two-photon detuning δ as a function of position z along the memory (normalized to length l) due to (i) the input gradient and (ii) output gradients, with minimum and maximum gradient offset δ_{os} (as noted on figure). The blue (dashed) line corresponds to the desired field, and points correspond to the measured magnetic field. (Error bars are due to the sensitivity of the Gauss meter.) (b) Heterodyne data showing (i) input pulse, (ii) echo for recall with $\delta_{os} = 0$, and (iii) echo for recall with $\delta_{os} = 1400$ kHz offset. Orange points correspond to raw data, black lines correspond to modulated Gaussian fit to data, and ω_c values correspond to the center frequencies of pulses extracted from the fits. (c) The change in the center frequency of the output pulses relative to the input pulse $\Delta\omega_c$ as a function of δ_{os}. Points represent the measured center frequency (error bars are from standard deviation of 100 traces), and the dashed line corresponds to the theoretical behavior.

With the MEC, we are able to vary the offset of the magnetic field down to tens of kHz precision, without altering the gradient. This fine control over the magnetic field is shown in Fig. 3(a), where (i) the input and (ii) output gradients for varying magnetic-field offsets are presented. As can be seen, the desired and measured magnetic fields are in close agreement.

Figure 3(b) shows single heterodyne traces for (i) input and (ii) echo with no applied offset, as well as (iii) echo with an applied offset of 1.4 MHz. While the frequency is shifted as we expect, there is also a substantial amount of pulse stretching, indicating that our pulses are subject to some dispersion in the memory. This is not surprising as the bandwidth of the memory is only slightly greater than the bandwidth of the pulse. Details of the dispersion in GEM can be found in Ref. [56], where the susceptibility has been explicitly calculated, clearly showing that, near the edges of the absorption window, there is great potential for slow light effects that will broaden recalled pulses. Having a larger memory input bandwidth would reduce the effect of dispersion on the pulse. The additional elongation for recall with a greater offset indicates that fringes of the magnetic field (i.e., those components that tail off at either end of the cell) may have affected the stored pulse, leading to greater dispersion. As we will explain in Sec. IV B, however, GEM provides a means to easily compensate for such pulse broadening.

A modulated Gaussian is fitted to the main body of the output pulses in order to extract the value of ω_c relative to the LO frequency. This is also shown in Fig. 3(b) for the input as well as for the two echoes. Figure 3(c) shows a characterization of the change in ω_c for a range of values of δ_{os}. This is compared with the behavior expected from Eq. (2). As can be seen, the two are in good agreement.

B. Bandwidth manipulation

By recalling with a steeper output gradient than input gradient, i.e., $|\eta(z, t > \tau)| > |\eta(z, t < \tau)|$, the output bandwidth of the memory $\mathcal{B}_o$ is made greater than the input bandwidth. This change in bandwidth is, in turn, passed on to the echo because the absolute emission frequency relative to the center frequency $|\omega(z) - \omega_c|$ of each atom along the ensemble will be greater, while the total excitation $\sigma_{12}(z, t)$ will remain unchanged. In this case, the output pulse will be compressed in time due to its now greater frequency spectrum. The opposite is also true: By recalling with a shallower gradient, the output pulse bandwidth will be reduced and the pulse elongated in time.

The temporal profile of the output pulse, measured using the pulse full width at half maximum (FWHM), $\mathcal{W}_o$, can be expressed as a function of the input profile $\mathcal{W}_i$ and input (output) gradient $\eta_{i/(o)}$ as

$$\mathcal{W}_o = \mathcal{W}_i|\eta_i/\eta_o|. \quad (3)$$

Again, it is the precise control of the MEC over the magnetic field that allows us to alter the bandwidth by tens of kHz without altering the offset. This is shown in Fig. 4(a), where experimental plots of (i) the input gradient and (ii) output gradients with ratios $|\eta_o/\eta_i|$ from 1:1 to 3:1 are shown. Performing fits to individual pulses, as illustrated in Fig. 3(b), allows for in-phase digital demodulation of the heterodyne data. This, in turn, allows for averaging over many traces, something that would not be possible with the nondemodulated data due to phase fluctuations between the probe and local oscillator.

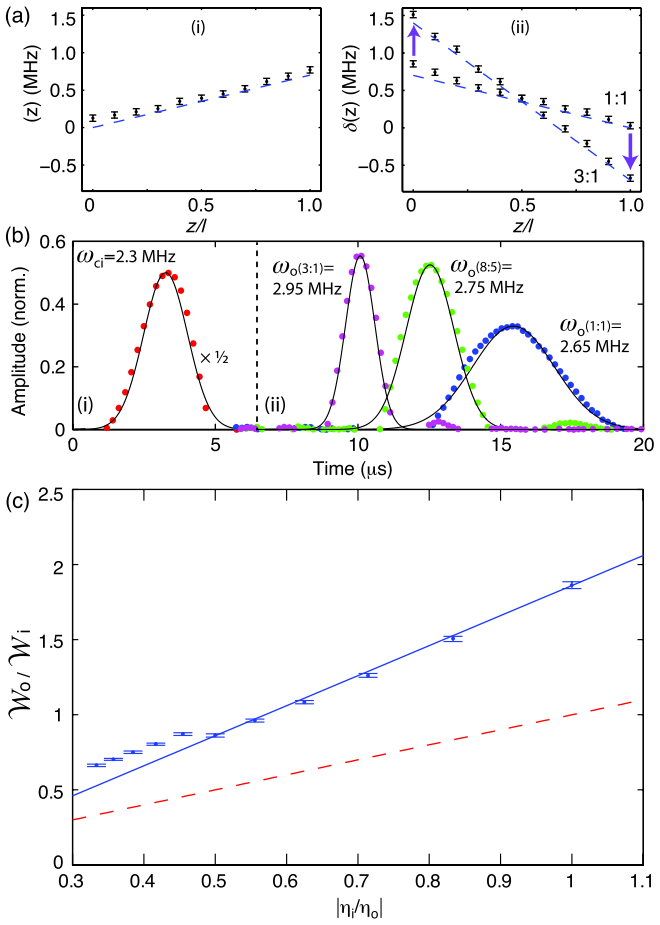

FIG. 4. Manipulating pulse bandwidth. (a) Two-photon detuning δ as a function of position z along the memory (normalized to length l) due to (i) the input gradient and (ii) minimum and maximum output gradients (ratios noted on figure). The blue (dashed) line corresponds to the desired field, and points correspond to the measured magnetic field. (Error bars are due to the sensitivity of the Gauss meter.) (b) Amplitude plot, normalized to the size of the input pulse, showing (i) the input pulse (in red, scaled by a factor of $1/2$) and (ii) output pulses recalled with varying output gradients as noted. Points correspond to demodulated data, lines correspond to Gaussian fit to data, and ω_c values correspond to the center frequencies of pulses relative to the LO. The bracketed ratios indicate η_o/η_i. (c) The FWHM of the output pulses $\mathcal{W}_o$ normalized to the FWHM of the input pulse $\mathcal{W}_i$, as a function of input gradient over output gradient $|\eta_i/\eta_o|$. Points represent measured FWHM (error bars are from standard deviation of 100 traces), the red (dashed) line corresponds to Eq. (3), and the blue (solid) line corresponds to a numerical simulation, with free parameters: $g = 0.066\ \mathrm{s}^{-1}$, $\gamma_0 = 0$, and $gN/c = 1000$.

Figure 4(b) shows averaged demodulated input and output pulse amplitudes for different recall gradients. As predicted, the output pulses become more compressed as the recall gradient is increased. Although it does follow a linear relationship, it does not, however, follow Eq. (3), as can be seen from Fig. 4(c). This discrepancy is more evidence of the dispersion that is present when the pulse bandwidth is approximately equal to the memory bandwidth, as it is in our experiment. Numerical modeling of the experiment with Eq. (1) and XMDS 2 simulations [59], using experimentally determined values for pulse and memory bandwidth parameters, also shows pulse broadening in excellent agreement with the experimental data. It can also be seen from Fig. 4(b) that the echoes are emitted from the memory earlier, i.e., at a time $t < 2\tau$, when recalled with a steeper output gradient. This is because a steeper gradient will cause the rephasing process to occur at a faster rate and will also reduce the amount of dispersion. The frequency of the echo is not the same as the input pulse due to the inherent GEM frequency shift predicted in Ref. [60], which is greater for shorter storage times.

C. Spectral filtering

If we now consider the storage of a modulated pulse, the frequency-encoding nature of GEM means that the carrier and sideband components of the pulse are stored in different parts of the memory. Therefore, if we had fine enough control over the recall gradient, we could choose when to recall the different frequency components by switching the gradient only in the pertinent part of the memory. The finer the control over the gradient, the greater the number of frequency components we can individually address.

An experimental demonstration of this filtering is shown in Figs. 5(a) and 5(b). Here, a carrier pulse with a Gaussian envelope and two frequency components separated by 700 kHz (the approximate bandwidth of the Gaussian) is sent into the memory. By reversing the gradient in only one half of the memory at a time, the different frequency components of the pulse can be recalled separately. The output pulses in this case both have the same ω_{co} due to the offset in the recall gradient for the lower-frequency component.

Furthermore, following the same logic, by being able to switch the gradient slowly along the length of the memory, the stored pulse can be recalled as its Fourier transform. This is shown experimentally in Figs. 5(c) and 5(d) for a modulated Gaussian with two sidebands at ± 700 kHz. In this case, the gradient is reversed in three stages, rather than a gradual reversal of the entire memory, due to the limitations of the LabVIEW code refresh rate (approximately 1 μs). The three outputs are fitted separately to allow for their different frequencies. The time window for each demodulation is denoted by the dashed vertical lines in Fig. 5(d).

In the above experimental demonstration, equal power is put into the sidebands and carrier. The reason this is not the case for the echo is because of the scattering of light induced by the coupling field. In normal Λ GEM storage, the coupling field is switched off during the storage process to limit this effect. Switching it off is not possible, however, for multipulse recall in a single gas cell as the coupling field must be present for recall to occur.

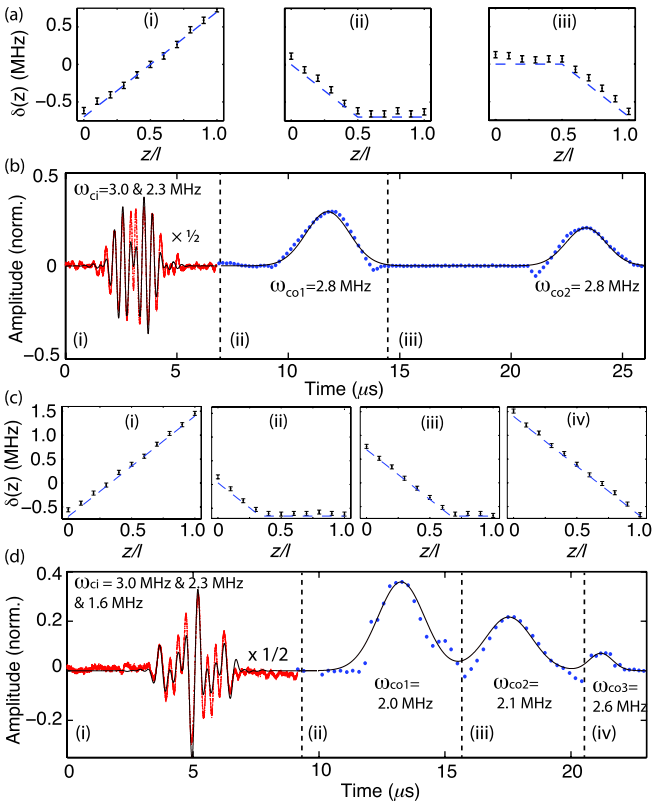

FIG. 5. Spectral filtering. (a) Two-photon detuning δ as a function of position z along the memory (normalized to length l) due to gradients (i)–(iii) corresponding to times (i)–(iii) in (b). For traces (a) and (c) blue (dashed) lines correspond to the desired field, and points correspond to the measured magnetic field. (Error bars are due to the sensitivity of the Gauss meter.) (b) Spectral filtering of (i) a Gaussian envelope containing two frequency components separated by 700 kHz (red, nondemodulated, scaled by $1/2$) and the demodulated retrieval (blue) of (ii) higher- and (iii) lower-frequency components averaged over 100 traces. For traces (b) and (d), points correspond to data, lines correspond to fit to data, and ω_c values correspond to center frequencies of pulses. (c) Two-photon detuning due to (i) input and (ii), (iii), and (iv) output gradients corresponding to times (i)–(iv) in (d), which shows the conversion from the time to the frequency domain of (i) a Gaussian pulse with two modulation sidebands at ± 700 kHz (red, nondemodulated, scaled by $1/2$), and the demodulated retrieval of (ii) the higher-frequency sideband, (iii) the carrier, and (iv) the lower-frequency sideband averaged over 100 traces (blue).

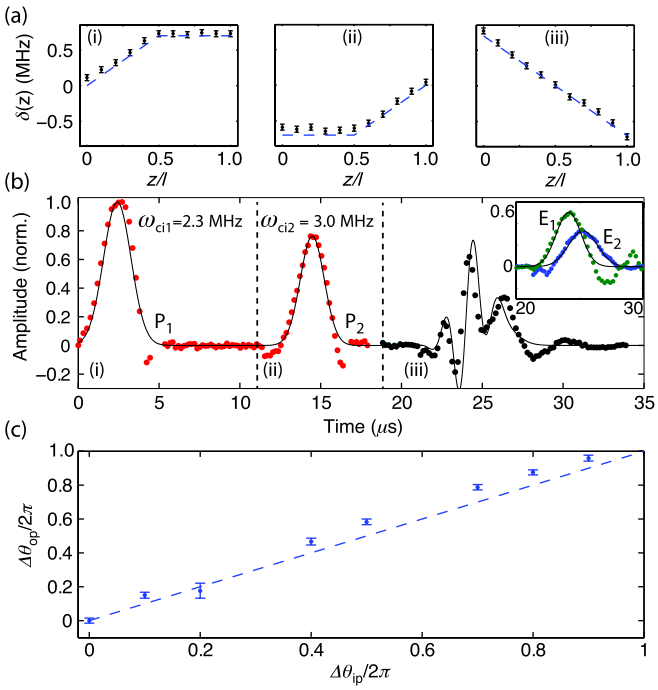

FIG. 6. Interference with pulses of different frequencies. (a) Two-photon detuning δ as a function of position z along the memory (normalized to length l) due to (i)–(ii) input gradients and (iii) the output gradient corresponding to times (i)–(iii) in (b). Blue (dashed) lines correspond to the desired field, and points correspond to the measured magnetic field. (Error bars are due to the sensitivity of the Gauss meter.) (b) Interference of two pulses that are initially time separated, (i) P_1 and (ii) P_2, shown in red, which are also separated in frequency by 700 kHz. Panel (iii) in (a) shows the superposition of the two pulses. The inset in (b) shows the output from the memory for storage of only a single pulse: P_1 recall (E_1, green) or P_2 recall (E_2, blue). Points correspond to demodulated data averaged over 100 traces, lines correspond to Gaussian fit to data, and ω_c values correspond to center frequencies of pulses. (c) The change in the relative phase of the fitted interference pulse $\Delta\theta_{op}$ as a function of the relative phase of the input pulses $\Delta\theta_{ip}$. Points represent data extracted from the fit (error bars are from standard deviation of 100 traces), and the dashed line corresponds to the theoretical behavior.

D. Pulse interference

A time reversal of the spectral filtering process is also possible. That is, if we take two pulses with different frequencies and store them one at a time in different halves of the memory, we can alter the gradients in the different halves at different times. This process causes the recalled echoes to overlap, and therefore interfere, at the output of the memory. Previous experiments in pulse interference using GEM have shown how the memory can facilitate interference between modes separated in either the time or the frequency domain [52]. In those cases, pulses were used to change the absorption and recall of other pulses since the light was being stored in the same part of the atomic ensemble. In our experiments, we use the MEC to separate the storage regions in space, allowing independent storage and recall of the modes.

Different frequency pulse interference is demonstrated in Figs. 6(a) and 6(b). Here, two pulses separated in frequency by 700 kHz are stored in separate halves of the memory, with the lower (higher) frequency pulse being stored in the second (first) half. Setting the gradient to 0 in the second half of the memory when the first (lower-frequency) pulse P_1 enters ensures that it will be stored in the first half of the memory. Setting the gradient to 0 in

the first half of the memory while the higher-frequency pulse P_2 enters and is stored serves two purposes: Apart from ensuring that none of P_2 is stored in the first half of the memory, it also means that the stored P_1 will not undergo any additional dephasing. Therefore, after P_2 is stored, we can reverse the gradient across the entire memory at once, causing the superposition of the echoes on the output.

To investigate the phase-preserving quality of the memory, we altered the relative phase between P_1 and P_2 and looked at the phase of the interference pattern of the echo. As can be seen from Fig. 6(c), the change in the relative phase of the two input pulses matches the relative phase of the interference pattern at the output. The only free parameter in the fitting of the echoes is the relative phase, with the amplitude, timings, and frequencies of the two individual pulses taken from the storage of individual echoes E_1 and E_2, shown in Fig. 6(b) (inset).

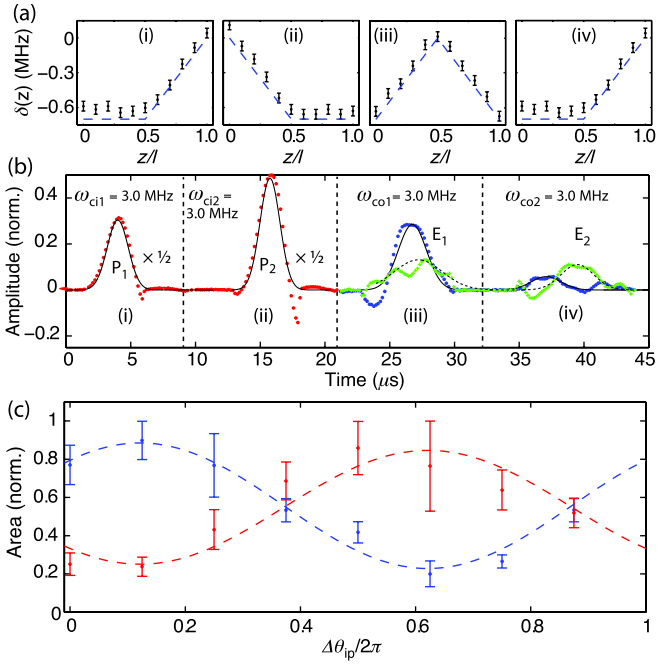

FIG. 7. Interference with pulses of the same frequency. (a) Two-photon detuning δ as a function of position z along the memory (normalized to length l) due to (i)–(ii) input gradients and (iii)–(iv) output gradients corresponding to times (i)–(iv) in (b). Blue (dashed) lines correspond to the desired field, and points correspond to the measured magnetic field. (Error bars are due to the sensitivity of the Gauss meter.) (b) Interference of two pulses, initially time separated, (i) P_1 and (ii) P_2 (red dashed lines), which have the same center frequency. (iii) Initial E_1, and (iv) secondary E_2 superpositions of the two pulses. Blue points and solid line correspond to maximum constructive interference for E_1, while green crosses and dashed line correspond to maximum constructive interference for E_2. Points correspond to demodulated data averaged over 100 traces, lines correspond to the Gaussian fit to the data, and ω_c values correspond to center frequencies of pulses. (c) The change in area (normalized to the maximum intensity of the individual echoes) as a function of the relative phase of the input pulses $\Delta\theta_{ip}$ for (i) E_1, and (ii) E_2. Points represent data extracted from the fit (error bars are from standard deviation of 100 fits), and the dashed line corresponds to a fit to the data.

Two pulses with the same frequency can also be caused to interfere in a similar manner. An experimental demonstration of same frequency interference is shown in Fig. 7. The two pulses are, as before, stored in different halves of the memory by setting $\eta = 0$ in the other half. As can be seen from Fig. 7(a)(iii), the first recall gradient is no longer monotonic and, therefore, the pulse stored in the first half of the memory, P_2, will be partly reabsorbed in the second half. This is why P_2 has a greater amplitude than P_1. The nonabsorbed component of P_2 will interfere with the retrieved light from the second part of the memory. If these two echoes are in phase, then there is constructive interference and an enhanced echo E_1 is retrieved. If they are out of phase, then E_1 will be small and the residual energy will remain as atomic excitation inside the memory. Therefore, if the gradient in the second half of the memory is switched again, a second echo E_2 can be recalled from the memory from these leftover excitations. This is shown in Figs. 7(b)(iii)–(iv).

Figure 7(c) shows the areas of the two echoes as the relative phase between P_1 and P_2 is varied. Interference fringes can be seen, with a π phase shift between the two echoes. The visibility for both E_1 and E_2 is approximately 60% (normalized to maximum echo output separately for E_1 and E_2). These values could potentially be improved with finer gradient control, especially in terms of timing.

V. DISCUSSION

In this paper, we have experimentally demonstrated a number of different spectral-manipulation operations using GEM. These operations could have various uses in a quantum information network. For instance, the ability to alter the bandwidth of the pulse, demonstrated in Sec. IV B, could be used to match systems with different bandwidths and, by increasing bandwidths, help to improve bit rates for a number of time-bin qubits, as described in [9]. Combining this use with the ability to change the center frequency of the stored information, as demonstrated in Sec. IV A, would allow one, in theory, to match any two optical systems.

This latter ability would allow for the conversion of time-bin qubits into frequency-bin qubits. It would also, along with the frequency-encoding nature of GEM, allow for frequency multiplexing. A number of pulses with different frequencies could be combined into one temporal pulse inside the memory, as demonstrated in Sec. IV D, and sent down the communication channel. Once the pulses reach the other end of the channel, they could be separated with a second memory, as demonstrated in Sec. IV C. This technique could greatly improve qubit rates over optical

channels in quantum information networks, as well as improve quantum-repeater protocols, as mentioned in Sec. I. It is worth mentioning also that this multiplexing is only possible with a memory that has the ability to both combine and separate multiple frequency components inside the memory into or from one temporal pulse. This ability is made possible by the precise control over the magnetic field provided by the MEC. It is not possible with the polaritonic interference techniques described in Ref. [52].

The phase-sensitive interference of pulses that are initially separated in time, demonstrated in Sec. IV D, could also find applications in quantum computing. In an all-optical switch, for instance, it is the relative phase between the pulses that determines how much light is emitted at different times [61].

All these potential applications require high efficiencies and therefore high-optical depths. A high-optical depth is especially important as increasing the bandwidth of the system decreases the recall efficiency. The pulse width for the above experiments was chosen to match the memory bandwidth in order to optimize efficiency. However, as seen in Secs. IV A and IV B this choice led to dispersion of the echoes. Being able to increase the memory bandwidth such that the pulse is absorbed away from the dispersive edges, as shown in modeling in Ref. [56], would significantly reduce this dispersion effect. If an increase in bandwidth is not possible, then a comprehensive characterization of the effect, like the one presented in Sec. IV B, will be required to make this operation useful.

A drawback to using one physical memory (i.e., the 20-cm-long gas cell) as a system of n submemories is that the optical depth for each individual submemory is $1/n$ of the total memory optical depth. An alternative method would be to use n physical memories placed in series to create a memory network. Not only would this technique increase the overall optical depth of the system, but it could help to alleviate two other drawbacks to the submemory approach taken here: the need for finer control of the gradient and the coupling-field-induced scattering.

Much care was taken with the design and construction of the multielement coil to allow for maximum precision in gradient creation with realistic currents. The MEC allows for separate control over the magnetic-field offset and bandwidth down to tens of kHz, something that is not possible with previous coil designs that were used to demonstrate proof of principle effects. The MEC allows us to characterize the bandwidth and frequency-manipulation properties of the memory. It also allows for individual storage and recall of up to three frequency components from the memory, limited by the resolution of the MEC. Using many physical memories as one memory network would automatically increase this resolution with respect to the length of each submemory. Another option for improving the resolution is to move to an alternate gradient-creation technique such as the ac Stark effect [62], which could allow for a much sharper change in the gradient by using, for instance, a spatial light modulator to create the intensity profile of the gradient field.

The coupling-field-induced scattering was discussed in Sec. IV C with regard to the extra decay of information that is left in the memory while other information is recalled. This decay is a concern, as this scattering leads to a decoherence rate almost 10 times larger than that presented by other decoherence mechanisms [3], and it cannot be combatted in a single memory. However, this issue could be addressed with a network of memories if one were to use orthogonal polarizations for the probe and coupling fields and to place polarizing beam splitters between the memories.

VI. CONCLUSIONS

In this paper, we have presented experimental demonstrations of theoretical spectral-manipulation operations originally investigated in Ref. [55]. With the introduction of a multielement coil to our memory protocol, we have characterized the gradient-echo-memory scheme's ability to alter the bandwidth (and therefore the temporal profile) of a pulse, as well as change its center frequency. We have also demonstrated the ability of GEM to act as a spectral filter, being able to separately address up to three separate frequency components stored in the memory and, using the frequency-encoding nature of GEM, were able to recall a modulated pulse as its Fourier transform. Finally, we showed that two pulses, initially time separated, with the same or different frequencies, could be caused to interfere coherently at the output of the memory. These abilities could be used to improve qubit rates across quantum communication channels, for instance, through frequency multiplexing, as well as to have potential uses in quantum-computing applications.

ACKNOWLEDGMENTS

The authors thank Shane Grieves for his work constructing the hardware for the MEC, and also Peter Uhe for his initial testing. This research was conducted by the *Australian Research Council Centre of Excellence for Quantum Computation and Communication Technology* (Project No. CE110001027).

[1] L.-M. Duan, M. D. Lukin, J. I. Cirac, and P. Zoller, *Long-Distance Quantum Communication with Atomic Ensembles and Linear Optics*, Nature (London) **414**, 413 (2001).

[2] A. I. Lvovsky, B. C. Sanders, and W. Tittel, *Optical Quantum Memory*, Nature Photon. **3**, 706 (2009).

[3] M. Hosseini, B. M. Sparkes, G. Campbell, P. K. Lam, and B. C. Buchler, *High Efficiency Coherent Optical Memory*

with Warm Rubidium Vapour, Nature Commun. **2**, 174 (2011).

[4] J. J. Longdell, E. Fraval, M. J. Sellars, and N. B. Manson, *Stopped Light with Storage Times Greater than One Second Using Electromagnetically Induced Transparency in a Solid*, Phys. Rev. Lett. **95**, 063601 (2005).

[5] R. Zhang, S. R. Garner, and L. V. Hau, *Creation of Long-Term Coherent Optical Memory via Controlled Nonlinear Interactions in Bose-Einstein Condensates*, Phys. Rev. Lett. **103**, 233602 (2009).

[6] K. F. Reim, J. Nunn, V. O. Lorenz, B. J. Sussman, K. C. Lee, N. K. Langford, D. Jaksch, and I. A. Walmsley, *Towards High-Speed Optical Quantum Memories*, Nature Photon. **4**, 218 (2010).

[7] E. Saglamyurek, N. Sinclair, J. Jin, J. A. Slater, D. Oblak, F. Bussières, M. George, R. Ricken, W. Sohler, and W. Tittel, *Broadband Waveguide Quantum Memory for Entangled Photons*, Nature (London) **469**, 512 (2011).

[8] M. Bonarota, J.-L. Le Gouët, and T. Chanelière, *Highly Multimode Storage in a Crystal*, New J. Phys. **13**, 013013 (2011).

[9] S. A. Moiseev and W. Tittel, *Temporal Compression of Quantum-Information-Carrying Photons Using a Photon-Echo Quantum Memory Approach*, Phys. Rev. A **82**, 012309 (2010).

[10] M. Brandt-Pearce, I. Jacobs, J.-H. Lee, and J. K. Shaw, *Optimal Input Gaussian Pulse Width for Transmission in Dispersive Nonlinear Fibers*, J. Opt. Soc. Am. B **16**, 1189 (1999).

[11] E. B. Treacy, *Optical Pulse Compression with Diffraction Gratings*, IEEE J. Quantum Electron. **5**, 454 (1969).

[12] H. P. Specht, J. Bochmann, M. Mücke, B. Weber, E. Figueroa, D. L. Moehring, and G. Rempe, *Phase Shaping of Single-Photon Wave Packets*, Nature Photon. **3**, 469 (2009).

[13] P. Kolchin, C. Belthangady, S. Du, G. Y. Yin, and S. E. Harris, *Electro-Optic Modulation of Single Photons*, Phys. Rev. Lett. **101**, 103601 (2008).

[14] B. H. Kolner, *Active Pulse Compression Using an Integrated Electro-optic Phase Modulator*, Appl. Phys. Lett. **52**, 1122 (1988).

[15] M. A. Dugan, J. X. Tull, and W. S. Warren, *High-Resolution Acousto-optic Shaping of Unamplified and Amplified Femtosecond Laser Pulses*, J. Opt. Soc. Am. B **14**, 2348 (1997).

[16] A. M. Weiner, *Femtosecond Pulse Shaping Using Spatial Light Modulators*, Rev. Sci. Instrum. **71**, 1929 (2000), and references therein.

[17] S. Viciani, A. Zavatta, and M. Bellini, *Nonlocal Modulations on the Temporal and Spectral Profiles of an Entangled Photon Pair*, Phys. Rev. A **69**, 053801 (2004).

[18] A. Pe'er, B. Dayan, A. A. Friesem, and Y. Silberberg, *Temporal Shaping of Entangled Photons*, Phys. Rev. Lett. **94**, 073601 (2005).

[19] B. Dayan, A. Pe'er, A. A. Friesem, and Y. Silberberg, *Two Photon Absorption and Coherent Control with Broadband Down-Converted Light*, Phys. Rev. Lett. **93**, 023005 (2004).

[20] B. H. Kolner and M. Nazarathy, *Temporal Imaging with a Time Lens*, Opt. Lett. **14**, 630 (1989).

[21] M. A. Foster, R. Salem, Y. Okawachi, A. C. Turner-Foster, M. Lipson, and A. L. Gaeta, *Ultrafast Waveform Compression Using a Time-Domain Telescope*, Nature Photon. **3**, 581 (2009).

[22] C. V. Bennett and B. H. Kolner, *Upconversion Time Microscope Demonstrating 103x Magnification of Femtosecond Waveforms*, Opt. Lett. **24**, 783 (1999).

[23] C. V. Bennet, R. P. Scott, and B. H. Kolner, *Temporal Magnification and Reversal of* 100 Gb/s *Optical Data with an Up Conversion Time Microscope*, Appl. Phys. Lett. **65**, 2513 (1994).

[24] J. Azaña, *Time-to-Frequency Conversion Using a Single Time Lens*, Opt. Commun. **217**, 205 (2003).

[25] M. T. Kauffman, W. C. Banyai, A. A. Godil, and D. M. Bloom, *Time-to-Frequency Converter for Measuring Picosecond Optical Pulses*, Appl. Phys. Lett. **64**, 270 (1994).

[26] H. J. McGuinness, M. G. Raymer, C. J. McKinstrie, and S. Radic, *Quantum Frequency Translation of Single-Photon States in a Photonic Crystal Fiber*, Phys. Rev. Lett. **105**, 093604 (2010).

[27] M. A. Foster, A. C. Turner, R. Salem, M. Lipson, and A. L. Gaeta, *Broad-Band Continuous-Wave Parametric Wavelength Conversion in Silicon Nanowaveguides*, Opt. Express **15**, 12949 (2007).

[28] D. Kielpinski, J. F. Corney, and H. M. Wiseman, *Quantum Optical Waveform Conversion*, Phys. Rev. Lett. **106**, 130501 (2011).

[29] B. Brecht, A. Eckstein, A. Christ, H. Suche, and C. Silberhorn, *From Quantum Pulse Gate to Quantum Pulse Shaper—Engineered Frequency Conversion in Nonlinear Optical Waveguides*, New J. Phys. **13**, 065029 (2011).

[30] A. Eckstein, B. Brecht, and C. Silberhorn, *A Quantum Pulse Gate Based on Spectrally Engineered Sum Frequency Generation*, Opt. Express **19**, 13770 (2011).

[31] M. T. Rakher, L. Ma, M. Davanço, O. Slattery, X. Tang, and K. Srinivasan, *Simultaneous Wavelength Translation and Amplitude Modulation of Single Photons from a Quantum Dot*, Phys. Rev. Lett. **107**, 083602 (2011).

[32] S. Ramelow, A. Fedrizzi, A. Poppe, N. K. Langford, and A. Zeilinger, *Polarization-Entanglement-Conserving Frequency Conversion of Photons*, Phys. Rev. A **85**, 013845 (2012).

[33] J. Huang and P. Kumar, *Observing of Quantum Frequency Conversion*, Phys. Rev. Lett. **68**, 2153 (1992).

[34] H. Takesue, *Single-Photon Frequency Down-Conversion Experiment*, Phys. Rev. A **82**, 013833 (2010).

[35] Y. Ding and Z. Y. Ou, *Frequency Downconversion for a Quantum Network*, Opt. Lett. **35**, 2591 (2010).

[36] A. P. VanDevender and P. G. Kwiat, *High-Speed Transparent Switch via Frequency Upconversion*, Opt. Express **15**, 4677 (2007).

[37] D. V. Vasilyev, I. V. Sokolov, and E. S. Polzik, *Quantum Memory for Images: A Quantum Hologram*, Phys. Rev. A **77**, 020302(R) (2008).

[38] C. Simon, H. de Riedmatten, M. Afzelius, N. Sangouard, H. Zbinden, and N. Gisin, *Quantum Repeaters with Photon Pair Sources and Multimode Memories*, Phys. Rev. Lett. **98**, 190503 (2007).

[39] O. A. Collins, S. D. Jenkins, A. Kuzmich, and T. A. B. Kennedy, *Multiplexed Memory-Insensitive Quantum Repeaters*, Phys. Rev. Lett. **98**, 060502 (2007).

[40] M. D. Eisaman, L. Childress, A. André, F. Massou, A. S. Zibrov, and M. D. Lukin, *Shaping Quantum Pulses of Light via Coherent Atomic Memory*, Phys. Rev. Lett. **93**, 233602 (2004).

[41] I. Novikova, N. B. Phillips, and A. V. Gorshkov, *Optimal Light Storage with Full Pulse-Shape Control*, Phys. Rev. A **78**, 021802(R) (2008).

[42] J. Wen, Y.-H. Zhai, S. Du, M. Xiao, *Engineering Biphoton Wave Packets with an Electromagnetically Induced Grating*, Phys. Rev. A **82**, 043814 (2010).

[43] A. W. Brown and M. Xiao, *All-Optical Switching and Routing Based on an Electromagnetically Induced Absorption Grating*, Opt. Lett. **30**, 699 (2005).

[44] S. A. Moiseev and B. S. Ham, *Photon-Echo Quantum Memory with Efficient Multipulse Readings*, Phys. Rev. A **70**, 063809 (2004).

[45] M. U. Staudt, S. R. Hastings-Simon, M. Nilsson, M. Afzelius, V. Scarani, R. Ricken, H. Suche, W. Sohler, W. Tittel, and N. Gisin, *Fidelity of an Optical Memory Based on Stimulated Photon Echoes*, Phys. Rev. Lett. **98**, 113601 (2007).

[46] G. Hétet, J. J. Longdell, A. L. Alexander, P. K. Lam, and M. J. Sellars, *Electro-Optic Quantum Memory for Light Using Two-Level Atoms*, Phys. Rev. Lett. **100**, 023601 (2008).

[47] A. L. Alexander, J. J. Longdell, M. J. Sellars, and N. B. Manson, *Coherent Information Storage with Photon Echoes Produced by Switching Electric Fields*, J. Lumin. **127**, 94 (2007).

[48] G. Hétet, M. Hosseini, B. M. Sparkes, D. Oblak, P. K. Lam, and B. C. Buchler, *Photon Echoes Generated by Reversing Magnetic Field Gradients in a Rubidium Vapor*, Opt. Lett. **33**, 2323 (2008).

[49] M. P. Hedges, J. J. Longdell, Y. Li, and M. J. Sellars, *Efficient Quantum Memory for Light*, Nature (London) **465**, 1052 (2010).

[50] M. Hosseini, G. Campbell, B. M. Sparkes, P. K. Lam, and B. C. Buchler, *Unconditional Room-Temperature Quantum Memory*, Nature Phys. **7**, 794 (2011).

[51] M. Hosseini, B. M. Sparkes, G. Hétet, J. J. Longdell, P. K. Lam, and B. C. Buchler, *Coherent Optical Pulse Sequencer for Quantum Applications*, Nature (London) **461**, 241 (2009).

[52] G. Campbell, M. Hosseini, B. M. Sparkes, P. K. Lam, and B. C. Buchler, *Time- and Frequency-Domain Polariton Interference*, New J. Phys. **14**, 033022 (2012).

[53] F. Carreño and M. A. Antón, *Coherent Control of Light Pulses Stored in a Gradient Echo Memory*, Opt. Commun. **284**, 3154 (2011).

[54] F. Carreño and M. A. Antón, *Gradient Echo Memory in a Tripod-Like Dense Atomic Medium*, Opt. Commun. **283**, 4787 (2010).

[55] B. C. Buchler, M. Hosseini, G. Hétet, B. M. Sparkes, and P. K. Lam, *Precision Spectral Manipulation of Optical Pulses Using a Coherent Photon Echo Memory*, Opt. Lett. **35**, 1091 (2010).

[56] M. Hosseini, B. M. Sparkes, G. T. Campbell, P. K. Lam, and B. C. Buchler, *Storage and Manipulation of Light Using a Raman Gradient Echo Process*, J. Phys. B **45**, 124004 (2012).

[57] A. V. Gorshkov, A. André, M. D. Lukin, and A. S. Sørensen, *Photon Storage in a Λ-Type Optically Dense Atomic Media. I. Cavity Model*, Phys. Rev. A **76**, 033804 (2007).

[58] B. M. Sparkes, H. M. Chrzanowski, D. P. Parrain, B. C. Buchler, P. K. Lam, and T. Symul, *A Scalable, Self-Analyzing Digital Locking System for Use on Quantum Optics Experiments*, Rev. Sci. Instrum. **82**, 075113 (2011).

[59] G. R. Dennis, J. J. Hope, and M. T. Johnsson, *XMDS2: Fast, Scalable Simulation of Coupled Stochastic Partial Differential Equations*, arXiv:1204.4255v1.

[60] S. A. Moiseev and N. M. Arslanov, *Efficiency and Fidelity of Photon-Echo Quantum Memory in an Atomic System with Longitudinal Inhomogeneous Broadening*, Phys. Rev. A **78**, 023803 (2008).

[61] S. E. Harris and Y. Yamamoto, *Photon Switching by Quantum Interference*, Phys. Rev. Lett. **81**, 3611 (1998).

[62] B. M. Sparkes, M. Hosseini, G. Hétet, P. K. Lam, and B. C. Buchler, *ac Stark Gradient Echo Memory in Cold Atoms*, Phys. Rev. A **82**, 043847 (2010).